Corresponding author: O. L. Konovalov
ORCID: 0009-0009-6367-4655
Email: konovalovol@bsu.by

PSI monitoring of fault zones at the Starobin potash deposit based on Sentinel-1 data

O. L. Konovalov[1], E. G. Shilkin[1]

[1]Belarusian State University,
Faculty of Applied Mathematics and Informatics,
Minsk, Belarus

konovalovol@bsu.by

ORCID: 0009-0009-6367-4655

Abstract

The Starobin potash salt deposit has been mined for over forty years with annual extraction measured in millions of tons. In the vicinity of tectonic fault junction zones, this creates a risk of local technogenic earthquakes caused by fault activation. Local geodetic monitoring within mining allotments is of limited utility for assessing large-scale tectonic deformations, since intense local technogenic subsidence masks the regional signal. Deploying a dense GPS network is economically and technically challenging. In this study, we test the applicability of Persistent Scatterer Interferometry (PSI) on Sentinel-1 data for large-scale geomechanical monitoring of fault zones. Processing was carried out on a stack of 12 SAR scenes (December 2020 – November 2021) using the SNAP–StaMPS environment for both ascending and descending tracks. Raw StaMPS LOS velocities in the Tanezhitsy/Chaplitsy area amounted to ∼30 mm/yr (ascending) and ∼10 mm/yr (descending). Verification against two GPS reference stations on the northern fault block (∼5 mm/yr, southwest) revealed a systematic overestimation of LOS velocities in the SNAP–StaMPS pipeline with a scaling factor $K_{\text{scale}} \approx 11.5$. A favorable circumstance — the near-collinear alignment of the ascending scan beam direction with the block displacement direction — enabled a simplified multiplicative calibration without full 3D decomposition. After calibration, corrected LOS velocities (2.6 mm/yr) are by construction consistent with the GPS reference. It is shown that, for the conditions of the Starobin deposit, the ascending and descending tracks exhibit different sensitivity to horizontal and vertical deformation components: the ascending track detects predominantly tectonic horizontal displacement, while the descending track captures vertical technogenic deformations. The geological interpretation indicates a strike-slip zone with a vertical component. Additionally, critical displacement zones of infrastructure objects were identified.

Keywords: PSI, Sentinel-1, persistent scatterer interferometry, fault zones, calibration, GPS verification, Starobin deposit, StaMPS.

1 Introduction

The Starobin potash salt deposit is mined by the joint-stock company "Belaruskali" using underground room-and-pillar methods since the 1960s. The annual extraction volume is measured in millions of tons; the total extraction over more than four decades has created an unprecedented technogenic load on the rock mass. Instrumental seismological monitoring since 1983 has recorded over 1,500 seismic events in the deposit area, including five felt earthquakes with magnitudes $M = 1.9$–3.1 [1]. The spatial distribution of epicenters extends beyond mine fields and is confined to tectonic faults, indicating induced seismicity caused by fault activation due to stress redistribution in the rock mass [2].

Monitoring ground surface deformation in fault junction zones is a critically important task for ensuring mining safety. The existing geodetic monitoring system is based on direct instrumental observations (leveling, GPS) within mining allotments [3]. However, this system has two fundamental limitations:

1. **Locality.** Intense local technogenic deformations (subsidence up to 0.5 cm/day above active workings) mask the large-scale tectonic signal in fault zones, where displacement rates are up to 1 cm/yr.

2. **Limited spatial coverage.** Deploying a dense large-scale GPS network for monitoring fault zones is economically and technically challenging.

An effective solution to the spatial coverage problem is satellite interferometry (InSAR) [4, 5]. Classical differential interferometry (DInSAR) is effective for high-speed subsidence processes (up to 2 cm/day) characteristic of active mining operations. The Sentinel-1 platform (ESA, Copernicus) provides free access to SAR data since 2014 and regular coverage of the deposit territory with a 10-day cycle and spatial resolution of 10–30 m [6]. For "slow" deformation processes in fault zones (rates up to 1 cm/yr), the Persistent Scatterer Interferometry (PSI) technique is most suitable [7, 8].

A known problem of PSI is the systematic scaling distortion of LOS velocities (LOS — Line-of-Sight, velocity along the scan beam), especially when using the open-source SNAP–StaMPS processing pipeline [13, 14]. The standard remedy for this distortion is calibration using subsatellite GPS survey data [15].

The objective of this study is to test the applicability of PSI for large-scale geomechanical monitoring of tectonic fault junction zones at the Starobin deposit and to develop a calibration methodology for PSI data using GPS reference stations. A key methodological advantage of the study area is the near-collinear alignment of the ascending scan beam direction of Sentinel-1 with the direction of horizontal block displacement, which enables a simplified multiplicative calibration without full 3D decomposition of LOS velocities.

2 Theoretical foundations of PSI

PSI utilizes time series of SAR images to isolate the deformation phase from the interferometric signal. The interferometric phase at a persistent scatterer point is expressed as:

$$\varphi_{\text{int}} = \varphi_{\text{def}} + \varphi_{\text{topo}} + \varphi_{\text{atm}} + \varphi_{\text{orbit}} + \varphi_{\text{noise}}, \tag{1}$$

where φ_{def} is the deformation phase, φ_{topo} is the residual topographic phase, φ_{atm} is the atmospheric phase screen, φ_{orbit} is the orbital phase error, and φ_{noise} is the decorrelation noise.

PSI measures deformation only at points where persistent scatterers exist (buildings, road surfaces, infrastructure). PS density is low in forested areas and agricultural lands [10]. PSI analysis in C-band requires a minimum of 15–20 SAR scenes over the same area [11]. The maximum measurable velocity for Sentinel-1 is 42.6 cm/yr.

3 Study area and data

3.1 Study area

The study area covers the mining allotment of the Krasnoslobodskoye mine directorate of JSC "Belaruskali" and includes the junction zone of the Northern and Krasnoslobodskoye tectonic faults, as well as the vicinity of the Kosynich fault. Two GPS reference stations are located near the settlements of Tanezhitsy (52°51′35″N, 27°39′41″E) and Chaplitsy (52°52′00″N, 27°40′43″E) — both on the northern fault block, which allows using this block as a reference for calibration.

Figure 1: Sentinel-1 data frame including the study area and GPS reference stations

The study zone is characterized by "slow" tectonic processes (up to 1 cm/yr), in contrast to high-speed technogenic subsidence (up to 0.5 cm/day) in active mining areas.

3.2 Satellite and GPS data

SAR data from Sentinel-1 (C-band, $\lambda = 5.6$ cm, IW mode, resolution 10–30 m) were used. A stack of 12 SLC scenes covering the period December 2020 – November 2021 was formed for both ascending and descending tracks. Data were downloaded via the ASF resource (https://search.asf.alaska.edu/).

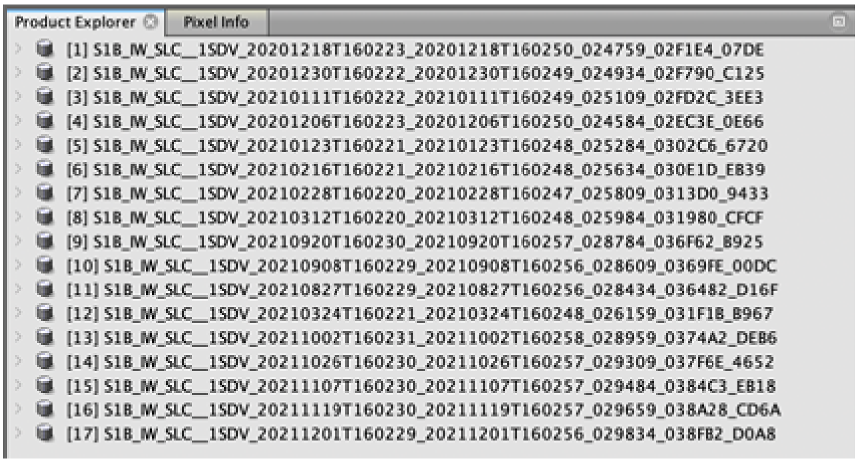

Figure 2: Stack of Sentinel-1 SAR scenes in SNAP

GPS observations at two reference stations on the northern block have been conducted over several years; the time interval of interest corresponds to the last segment of the displacement trajectory.

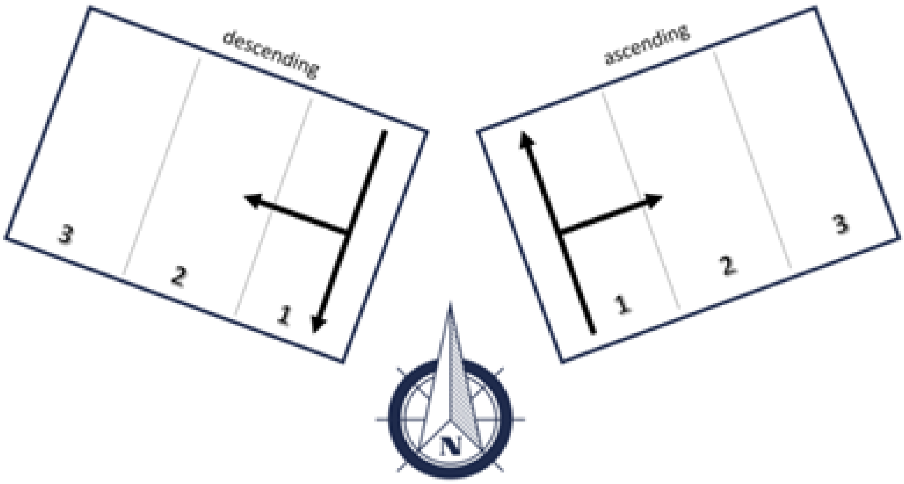

Figure 3: Scan directions for descending and ascending Sentinel-1 tracks

4 Methods

4.1 SNAP–StaMPS processing

PSI processing was performed in the integrated SNAP–StaMPS environment [12] (Linux, MATLAB). The processing sequence: coregistration of scenes to a master image, interferogram generation, PS candidate selection using the amplitude dispersion index, temporal and spatial phase unwrapping (3D unwrapping), velocity and residual topographic error estimation, geocoding. Visualization was done through the GeoServer mapping server.

4.2 LOS velocity and calibration

The LOS velocity is related to the displacement vector $\mathbf{v} = (v_E, v_N, v_U)$ by:

$$v_{\text{LOS}} = v_U \cos\theta - v_E \sin\theta \cos\alpha + v_N \sin\theta \sin\alpha, \tag{2}$$

where $\theta \approx 39^\circ$ is the incidence angle (from vertical), $\alpha \approx -11^\circ$ is the satellite heading azimuth (ascending orbit). A positive v_{LOS} value corresponds to motion away from the satellite (subsidence).

Key assumption. The direction of horizontal block displacement (southwest, azimuth $\approx 225^\circ$) is nearly collinear with the ascending track scan beam direction. This allows using Eq. (2) to project the GPS vector onto LOS and apply a multiplicative calibration without full 3D decomposition.

5 PSI results

5.1 Interferogram time series and PS distribution

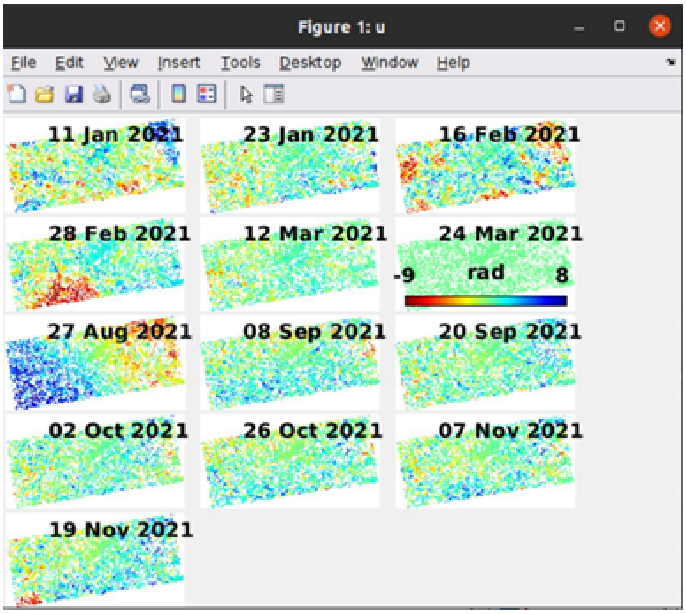

Figure 4: Time series of pairwise differential interferograms (PSI processing of the Sentinel-1 stack)

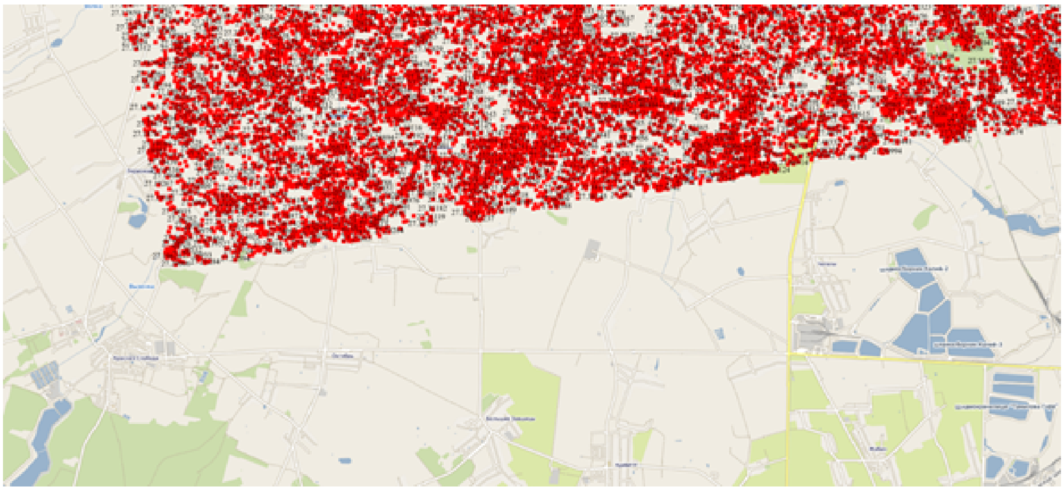

Figure 5: Distribution of persistent scatterers (GeoServer)

Phase centers of PS are associated with road surfaces, railway tracks, building roofs, and elevated terrain features — objects with stable radar reflectivity.

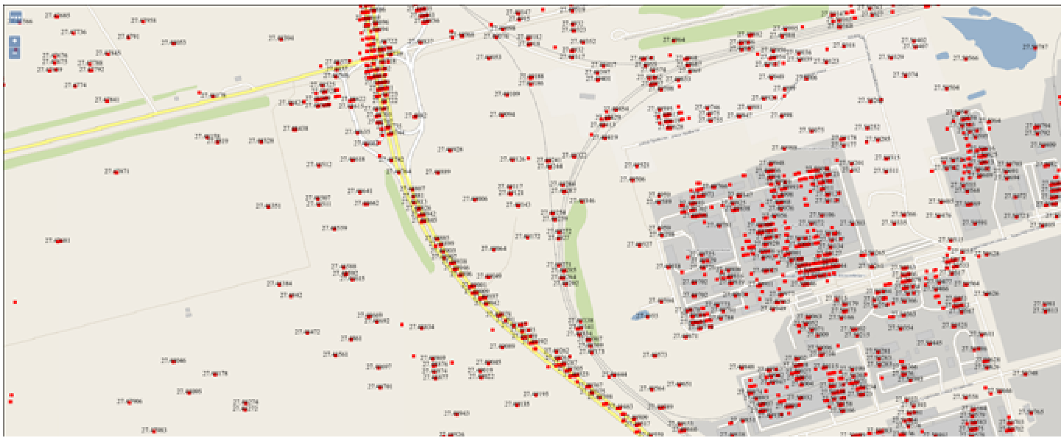

Figure 6: PS distribution near the Slutsk bypass road

5.2 Annual LOS velocities

Fig. 7 shows annual LOS velocities (ascending track, uncalibrated StaMPS values) in the Tanezhitsy/Chaplitsy area. Positive values (blue points) correspond to subsidence; negative values (yellow points) to uplift.

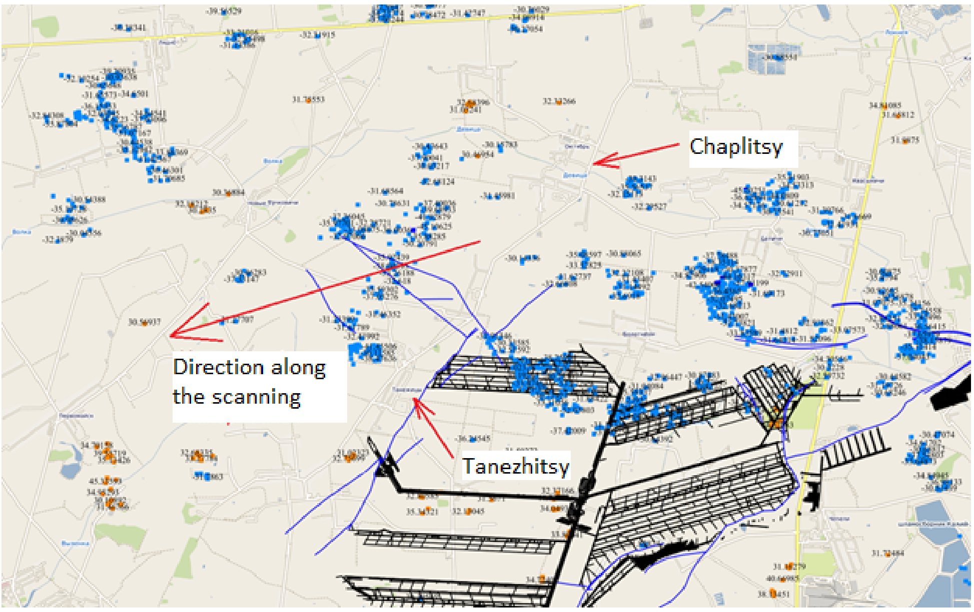

Figure 7: Annual LOS velocities of PS in the Tanezhitsy/Chaplitsy area (ascending track)

Raw StaMPS LOS velocities amounted to ∼30 mm/yr (ascending) and ∼10 mm/yr (descending). The significant contrast between tracks indicates that the horizontal displacement vector is close to the ascending track scan beam direction.

5.3 Additional displacement zones

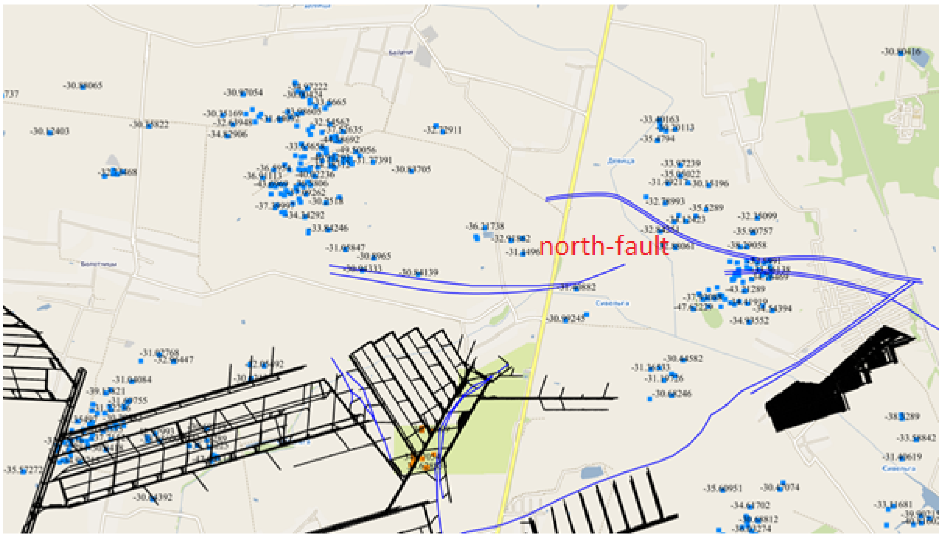

Figure 8: Displacement velocities near the Northern fault

[FIGURE]

Displacement velocities near the railway tracks and the bridge over the Sivelga River

File: `figures/fig-railway-bridge.png`

Figure 9: Displacement velocities near the railway tracks and the bridge over the Sivelga River

PSI analysis revealed significant displacements in several zones: the Northern fault (southwestward), the South-Kosynich fault (northeastward), the Central fault (vertical component on descending track), as well as critical velocities near the railway tracks of mine directorate No. 3 and the bridge over the Sivelga River (westward) — a potential infrastructure risk.

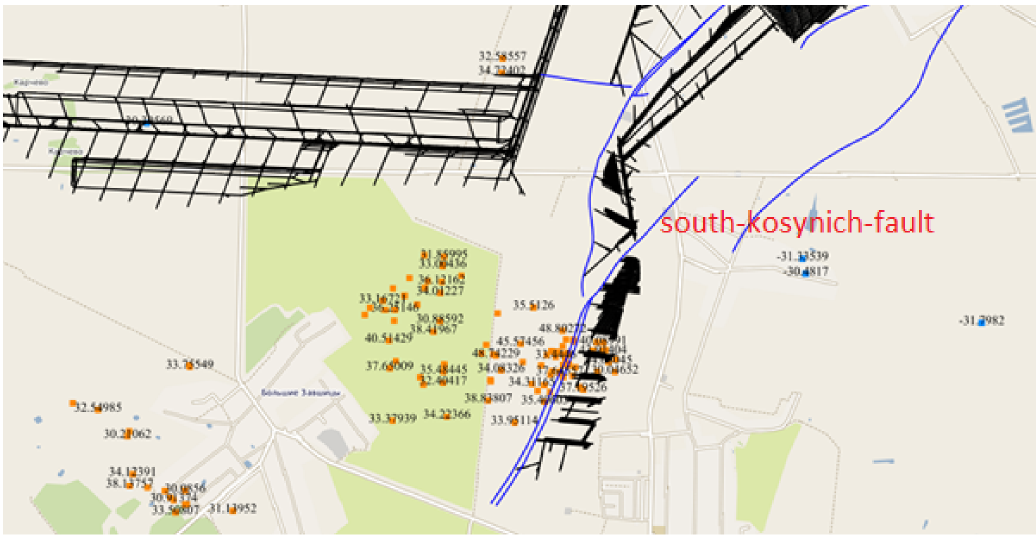

Figure 10: Displacement velocities: South-Kosynich fault

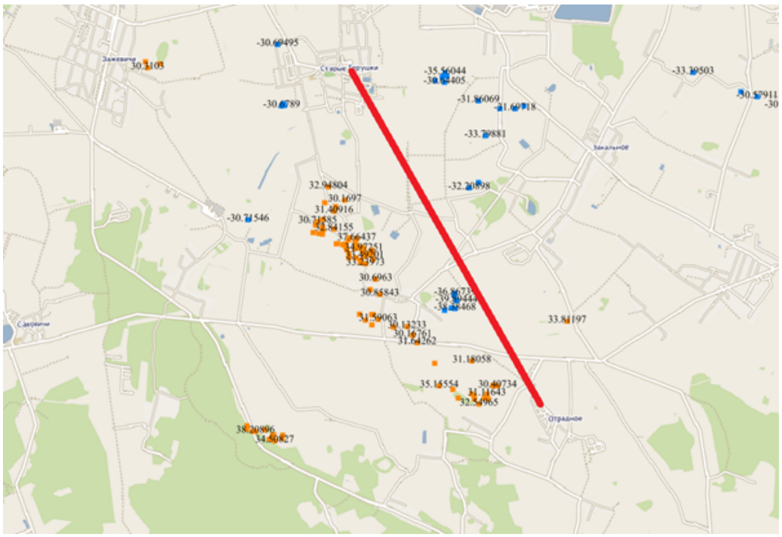

Figure 11: Velocities along the Otradnoye – Staryye Terushki line (ascending)

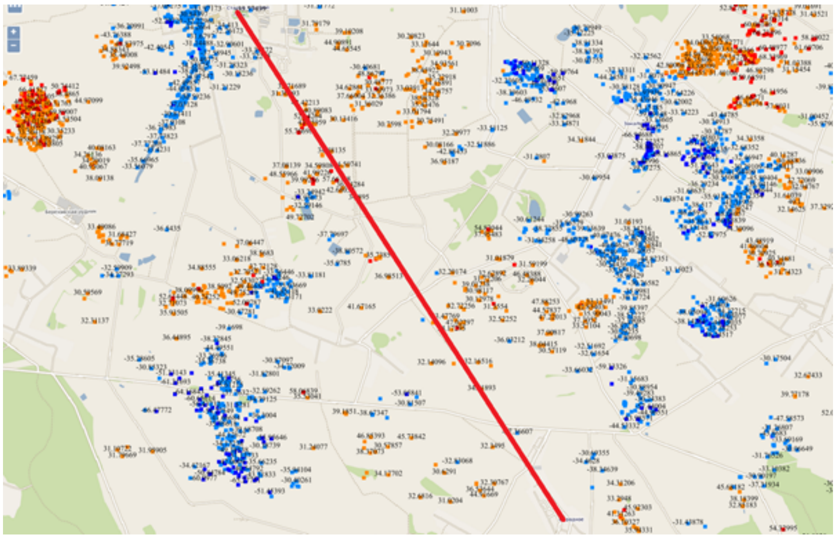

Figure 12: Velocities along the Otradnoye – Staryye Terushki line (descending)

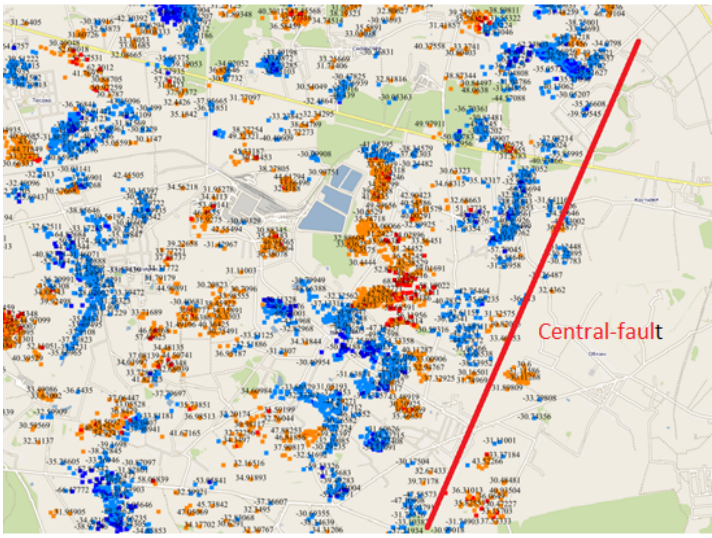

Figure 13: Descending track velocities, Central fault

6 GPS calibration and verification

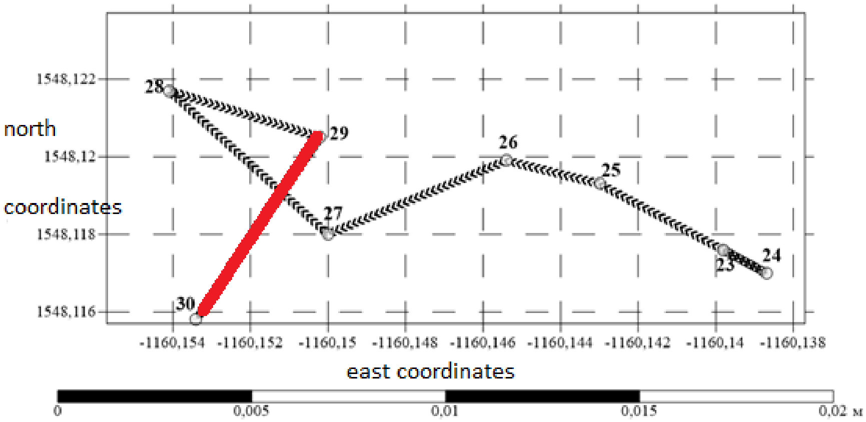

Figure 14: Displacement trajectory of GPS reference station 2 (Tanezhitsy)

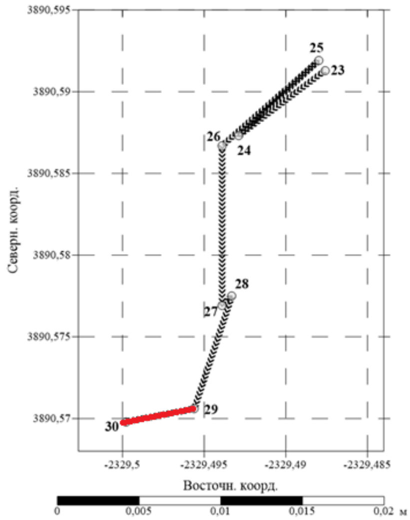

Figure 15: Displacement trajectory of GPS reference station 3 (Chaplitsy)

Both GPS reference stations, located on the northern fault block, record horizontal displacement at a rate of ∼5 mm/yr in the southwest direction. The vector components are: $v_E = v_N = -5/\sqrt{2} = -3.54$ mm/yr, $v_U = 0$.

Projection of the GPS vector onto the ascending LOS using Eq. (2) with $\theta = 39°$, $\alpha = -11°$:

$$\begin{aligned} v_{\text{LOS}}^{\text{GPS}} &= 0 \cdot \cos\theta - (-3.54) \cdot \sin\theta \cdot \cos\alpha + (-3.54) \cdot \sin\theta \cdot \sin\alpha \\ &= 3.54 \cdot \sin 39° \cdot \left[\cos 11° + \sin 11°\right] \\ &= 3.54 \cdot 0.629 \cdot 1.172 \approx 2.61 \text{ mm/yr.} \end{aligned} \tag{3}$$

Comparison with raw StaMPS values along the ascending track near the GPS reference stations (∼30 mm/yr) reveals a systematic overestimation. The scaling factor is determined as the ratio of the raw PSI velocity to the theoretical GPS projection:

$$K_{\text{scale}} = \frac{v_{\text{LOS}}^{\text{raw}}}{v_{\text{LOS}}^{\text{GPS}}} = \frac{30}{2.61} \approx 11.5. \tag{4}$$

This overestimation is likely caused by software artifacts in the SNAP–StaMPS pipeline: when processing large areas, the `stamps_export` scripts may incorrectly translate the pixel spacing into StaMPS binary matrices, leading to a multiple distortion of the phase gradient [13, 14].

The multiplicative calibration:

$$v_{\text{final}} = \frac{v_{\text{raw}}}{K_{\text{scale}}} \tag{5}$$

by construction yields, at the GPS reference stations, a corrected LOS velocity exactly equal to the theoretical projection $v_{\text{LOS}}^{\text{GPS}} = 2.61$ mm/yr. Given the key assumption that the displacement direction coincides with the ascending beam, the true horizontal tectonic displacement rate is ∼5 mm/yr.

7 Kinematics of the fault zone

The difference in spatial morphology of displacement patterns between the ascending and descending tracks is a direct consequence of scan geometry and confirms the differentiated nature of deformations.

7.1 Ascending track: horizontal tectonic displacement

On the ascending track, the beam is directed east-northeast (look azimuth $\approx 78.6°$). The tectonic displacement vector (southwest, azimuth $\approx 225°$) is nearly collinear with the line of sight, giving the ascending track maximum sensitivity to the horizontal component. On velocity maps, large crustal blocks separated by the fault line are clearly delineated — these are regional displacements verified by GPS ($\sim$5 mm/yr after calibration).

7.2 Descending track: vertical technogenic deformations

On the descending track, the beam is directed nearly mirror-opposite (look azimuth $\approx 251.4°$). The horizontal tectonic signal is partially compensated for this geometry, and the dominant signal becomes vertical technogenic deformation: local subsidence from salt dumps, tailings ponds, and mining subsidence troughs. As a result, the block structure disappears on the descending track, replaced by a mosaic ("patchy") anomaly morphology spatially associated with industrial infrastructure objects.

7.3 Argument in support of calibration

If the raw $\sim$30 mm/yr on the ascending track were the real horizontal displacement rate, the descending track should show comparable block structures with inverted LOS sign. However, the descending track shows no block structures — only small local patches. This proves that the real tectonic signal is small ($\sim$2.6 mm/yr in LOS), and on the descending track it "drowned" against the background of local technogenic noise. The scaling factor $K_{\text{scale}} \approx 11.5$ is physically justified.

7.4 Geological interpretation

The northern block (reference) is displaced to the southwest ($\sim$5 mm/yr). The southern block exhibits positive LOS velocities (after calibration — a few mm/yr), corresponding to eastward and/or upward motion. Interpretation depends on the contribution of components:

- **Pure sinistral strike-slip**: northern block moves west, southern block moves east. However, eastward displacement gives a negative LOS contribution for the ascending orbit, while a positive value is observed. A purely horizontal model is insufficient.
- **Strike-slip with vertical component**: the southern block moves east and simultaneously rises ($v_U > 0$). The vertical component gives a positive contribution $v_U \cos\theta$ ($\approx 0.78\, v_U$) that can exceed the negative contribution of eastward displacement, consistent with observations.

Thus, the geological model suggests a **strike-slip zone with a vertical component** (sinistral strike-slip complicated by uplift of the southern block), consistent with the technogenic impact of underground mining on the stress state of the rock mass.

8 Discussion

After multiplicative calibration, the corrected PSI velocities at the GPS reference stations are by construction equal to the theoretical GPS projection ($v_{\text{LOS}}^{\text{GPS}} = 2.61$ mm/yr).

The calibration accuracy over the rest of the territory depends on the spatial homogeneity of the scaling distortion. Possible sources of inhomogeneity:

1. **Unresolved vertical component**: in zones where the vertical displacement component is nonzero (e.g., the southern block, see Section 7), the scaling factor may differ from K_{scale} determined on the horizontal reference block.

2. **Atmospheric and orbital residuals**: uncompensated low-frequency atmospheric effects can introduce spatially varying systematic tilts in velocity maps. A tilt may be falsely interpreted as a geophysical signal, or, conversely, a real low-frequency signal may be removed along with atmospheric residuals.

3. **Short observation period**: 12 scenes over one year is the minimum acceptable dataset for PSI; extending the period would improve the signal-to-noise ratio.

Comparison with published PSI verification data shows that under optimal conditions (large data volumes, high PS density, low velocities), the typical discrepancy with independent measurements is 0.5–3 mm/yr [16, 17, 18, 19]. The overestimation we detected ($K_{scale} \approx 11.5$) substantially exceeds these values, explained by the use of the open-source SNAP–StaMPS pipeline, in which the scaling artifact is systematic in nature. This problem can be partially overcome by combining PSI with external GPS data, as done in this study, and by using multiple overlapping tracks.

9 Conclusion

1. PSI on Sentinel-1 data is applicable for large-scale geomechanical monitoring of fault zones at the Starobin deposit, provided GPS-based calibration is applied.

2. A systematic overestimation of LOS velocities in the SNAP–StaMPS pipeline was identified with a scaling factor $K_{scale} \approx 11.5$. Multiplicative calibration using two GPS stations on the northern fault block yields a corrected LOS velocity of 2.61 mm/yr, exactly equal to the theoretical projection of the GPS vector onto the scan beam. The true horizontal tectonic displacement rate is $\sim$5 mm/yr.

3. The near-collinear alignment of the ascending scan beam with the block displacement direction simplifies calibration (multiplicative only) and the algorithm for extracting the horizontal component from LOS.

4. For the conditions of the Starobin deposit, the ascending and descending tracks exhibit different sensitivity to horizontal and vertical deformation components: the ascending track is a detector of tectonic horizontal displacement, while the descending track is an indicator of vertical technogenic deformations (salt dumps, tailings ponds, mining subsidence troughs).

5. The geological interpretation indicates a strike-slip zone with a vertical component (sinistral strike-slip complicated by uplift of the southern block).

6. Critical displacement zones of infrastructure objects were identified — the railway tracks of mine directorate No. 3 and the bridge over the Sivelga River.

Future research: extending the observation period, joint use of ascending and descending orbits for full 3D decomposition, integration with numerical geomechanical models, and development of an automated processing pipeline for near-real-time monitoring.

Acknowledgments

This work was supported by the State Program of Scientific Research of the Republic of Belarus (SPSR "Digital and Space Technologies, Human, Society and State Security" 2021–2025, Subprogram 1, Task 1.7.1.1). The authors thank the European Space Agency (ESA) for providing Sentinel-1 SAR data via the Copernicus portal and the ASF (Alaska Satellite Facility) resource.

References

[1] Aronov A.G., Aronov G.A. Monitoring of induced seismicity in the Starobin potash salt deposit region of Belarus // NNC RK Bulletin. 2018. No. 2. P. 129–134. (in Russian)

[2] Aronov A.G., Mukhamediev Sh.A., Aronova T.I. Seismicity and the stressed state of the Starobin potassium salt deposit in Belarus // Geodynamics. 2014. No. 1(16). P. 88–95.

[3] Kozlovskiy E.Ya., Zhuravkov M.A. Determination and verification of parameters of a computational model of salt rocks accounting for softening and creep // Journal of Mining Institute. 2021. Vol. 247. P. 33–38. DOI: 10.31897/PMI.2021.1.4

[4] Ferretti A., Prati C., Rocca F. Nonlinear subsidence rate estimation using permanent scatterers in differential SAR interferometry // IEEE Trans. Geosci. Remote Sens. 2000. Vol. 38, No. 5. P. 2202–2212.

[5] Ferretti A., Prati C., Rocca F. Permanent scatterers in SAR interferometry // IEEE Trans. Geosci. Remote Sens. 2001. Vol. 39, No. 1. P. 8–20.

[6] Torres R., Snoeij P., Geudtner D., et al. GMES Sentinel-1 mission // Remote Sens. Environ. 2012. Vol. 120. P. 9–24.

[7] Crosetto M., Monserrat O., Cuevas-González M., et al. Persistent scatterer interferometry: A review // ISPRS J. Photogramm. Remote Sens. 2016. Vol. 115. P. 78–89.

[8] Osmanoglu B., Dixon T.H., Wdowinski S., et al. Mexico City subsidence observed with persistent scatterer InSAR // Int. J. Appl. Earth Obs. Geoinf. 2011. Vol. 13, No. 1. P. 1–12.

[9] Berardino P., Fornaro G., Lanari R., Sansosti E. A new algorithm for surface deformation monitoring based on small baseline differential SAR interferograms // IEEE Trans. Geosci. Remote Sens. 2002. Vol. 40, No. 11. P. 2375–2383.

[10] Kampes B.M. Radar Interferometry: Persistent Scatterer Technique. Dordrecht: Springer, 2006. 211 p.

[11] Hooper A., Bekaert D., Spaans K., Arıkan M. Recent advances in SAR interferometry time series analysis for measuring crustal deformation // Tectonophysics. 2012. Vol. 514–517. P. 1–13.

[12] Hooper A., Bekaert D., Spaans K. StaMPS/MTI Manual. Version 4.1b, 2018. https://homepages.see.leeds.ac.uk/~earahoo/stamps/

[13] Foumelis M., Delgado Blasco J.M., Desnos Y.L., et al. ESA SNAP–StaMPS integrated processing for Sentinel-1 persistent scatterer interferometry // IEEE IGARSS 2018. P. 1364–1367. DOI: 10.1109/IGARSS.2018.8519545

[14] Delgado Blasco J.M., Foumelis M., Stewart C., Hooper A. Open-source software package for automated Sentinel-1 PSI processing: snap2stamps // IEEE IGARSS 2019. P. 8914–8917. DOI: 10.1109/IGARSS.2019.8849035

[15] Mancini F., Grassi F., Cenni N. A workflow based on SNAP–StaMPS open-source tools and GNSS data for PSI-based ground deformation using dual-orbit Sentinel-1 data: accuracy assessment with error propagation analysis // Remote Sens. 2021. Vol. 13, No. 4. Art. 753. DOI: 10.3390/rs13040753

[16] Ferretti A., Savio G., Barzaghi R., et al. Submillimeter accuracy of InSAR time series: experimental validation // IEEE Trans. Geosci. Remote Sens. 2007. Vol. 45, No. 5. P. 1142–1153.

[17] Marinkovic P., Ketelaar G., van Leijen F., Hanssen R. InSAR quality control: analysis of five years of corner reflector time series // Proc. FRINGE 2007. Frascati, Italy, 2007.

[18] Musson R.M., Haynes M., Ferretti A. Space-based tectonic modeling in subduction areas using PSInSAR // Seismol. Res. Lett. 2004. Vol. 75, No. 5. P. 598–606.

[19] Casu F., Manzo M., Lanari R. A quantitative assessment of the SBAS algorithm performance for surface deformation retrieval from DInSAR data // Remote Sens. Environ. 2006. Vol. 102, No. 3. P. 195–210.

[20] Hooper A., Segall P., Zebker H. Persistent scatterer InSAR for crustal deformation analysis, with application to Volcán Alcedo, Galápagos // J. Geophys. Res. 2007. Vol. 112, No. B7. DOI: 10.1029/2006JB004763